

Article

A Study of PbF₂ Nanoparticles Crystallization Mechanism in Mixed Oxide-Fluoride Glasses

Saule Dyussembekova^{1,2}, Ekaterina Trusova^{3,*} , Sergey Kichanov¹ , Kiril Podbolotov⁴  and Denis Kozlenko¹¹ Frank Laboratory of Neutron Physics, Joint Institute for Nuclear Research, 141980 Dubna, Russia² Institute of Nuclear Physics, Ministry of Energy of the Republic of Kazakhstan, Almaty 050032, Kazakhstan³ Glass and Ceramics Technology Department, Belarusian State Technological University, 220006 Minsk, Belarus⁴ State Scientific Institution "The Physical-Technical Institute of the National Academy of Sciences of Belarus", 220141 Minsk, Belarus

* Correspondence: trusova@belstu.by; Tel.: +375-297674337

Abstract: Samples of nanocrystalline PbF₂ glass ceramics were obtained by heat-treating SiO₂–GeO₂–PbO–PbF₂–CdF₂ glasses. The Ho₂O₃ and Tm₂O₃ doping effects on the structural features of PbF₂ nanoparticles were studied using small-angle X-ray scattering and X-ray diffraction methods. The enlargements of the average sizes of nanoparticles and the sizes of local areas of density fluctuations have been found to be correlated with an increase in concentrations of Ho₂O₃ and Tm₂O₃ in initial glasses. A variation in the concentrations of Ho₂O₃ and Tm₂O₃ does not affect the morphology and fractal dimension of the formed PbF₂ nanoparticles.

Keywords: oxyfluoride glasses; glass ceramics; small-angle X-ray scattering; nanoparticles



Citation: Dyussembekova, S.; Trusova, E.; Kichanov, S.; Podbolotov, K.; Kozlenko, D. A Study of PbF₂ Nanoparticles Crystallization Mechanism in Mixed Oxide-Fluoride Glasses. *Ceramics* **2023**, *6*, 1508–1516. <https://doi.org/10.3390/ceramics6030093>

Academic Editor: Georgiy Shakhgildyan

Received: 21 May 2023

Revised: 2 July 2023

Accepted: 4 July 2023

Published: 11 July 2023



Copyright: © 2023 by the authors. Licensee MDPI, Basel, Switzerland. This article is an open access article distributed under the terms and conditions of the Creative Commons Attribution (CC BY) license (<https://creativecommons.org/licenses/by/4.0/>).

1. Introduction

Fine-tuning the optical properties of glass ceramics with embedded optical nanoparticles, as well as synthesizing novel vitreous composite materials, can extend their applicability and functionality and show novel methods for their technical applications [1,2]. Transparent glass ceramic materials [1–5] are widely used to increase the efficiency of solar cells as near-infrared light sources, in optical glass fibers and sensors and in elements for laser technology [6,7]. First of all, this is due to the formation of non-linear optical properties [2,8,9] in glass-based materials. Their chemical and thermal stability, and ability to finely control the optical properties and structural characteristics of nanoparticles during synthesis, were reported [5,10,11].

Rare-earth (RE) ions are optically active elements that are sources of effective luminescence, and nanoparticles doped with these ions are characterized by high quantum yields, wide possibilities of tuning optical properties, and noticeable suppression of the effect of concentration quenching [12]. Therefore, luminescent glasses and glass ceramics based on rare-earth ions with a stoichiometric or non-stoichiometric composition are a promising replacement for phosphor single crystals [13].

The formation of predominantly amorphous PbF₂ nanoparticles and clusters in the glass matrix is observed [5,14]. The nanoparticles form complex fractal-like structures consisting of semi-regular arrangements that resemble concentration bunches inside the glass material. The PbF₂ nanoparticles doped with different RE ions embed well in a glass matrix, which is a source of their optical properties, and greatly enhances the emission yields of the corresponding optical materials. The PbF₂ nanoparticles are clustered in complex aggregates of sizes 10–30 nm [5]. Recently, it was shown that PbF₂ nanoparticles can be doped with RE ions up to a high doping level of 10 wt.% without luminescence yield losses [15]. The optically active nanoparticles could be formed based on the density fluctuations in the glasses, which can definitely affect the structural properties of the PbF₂ nanoparticles. Moreover, the glasses and associated glass fibers doped with RE ions have

certain advantages, such as a low melting temperature [5] and high ultraviolet resistance. From this point of view, the up-conversion luminescent glass ceramics with PbF₂ nanoparticles are of particular interest [15–18]. These glass materials have potential applications in the fields of emission displays, cathode-ray tubes and solid-state lighters. The phenomenon of up-conversion luminescence is the joint radiation of a multicomponent system through sequential optical transitions between various optically active ions [14–21]. Thus, as an example, one can cite the processes of up-conversion luminescence of PbF₂ nanoparticles doped with Yb³⁺ and Eu³⁺ ions, in which the emission of infrared radiation is observed during optical pumping of Yb³⁺ ions from the energy levels of Eu³⁺ ions [18–20]. During the high-temperature treatment, crystallization of the nanoparticles of PbF₂ from concentration bunches exists [14]. The crystalline nanoparticles are host systems for rare earth elements that provide the conditions for up-conversion luminescence [18]. At the same time, the growth and uniform distribution of these nanoparticles inside the glasses are proposed. The uniform distribution of nanoparticles is the reason for the suppression of the concentration luminescence quenching characteristic of large clusters of nanoparticles [5,14,17]. Both the crystallization and uniform distribution of nanoparticles determine the high intensity of luminescence observed in the glasses. The combination of RE ions as joint activators of optical centers with up-conversion luminescence excitation mechanisms enhances the optical properties of the glass ceramics [15,18].

For transparent glass ceramic materials, the efficiency of up-conversion luminescence depends not only on the type and concentration of optically active RE ions but also on the type and composition of the glass matrix [5,10,14,18], the chemical nature of the formed nanoparticles, and thermal treatment modes [14]. It should be noted that an important problem in the development of glass-nanoceramics is the optimization of the glass composition, which has effects on the spectral–optical properties of the system. Furthermore, the stability of the glass materials is required when introducing fluorides and oxides of RE elements with a molar concentration of a few percent [3,16,17]. Recently, interest in the studies of oxyfluoride and germanium–gallium glasses doped with thulium and holmium ions has grown [19,21,22]. These ions have optical transitions in the infrared region with a high energy transfer efficiency of the Tm³⁺-Ho³⁺ process during up-conversion luminescence. The presence of holmium ions in glass nanoceramics makes these materials promising for infrared laser sources with a wavelength of 2 μm [21]. Currently, much attention is paid to optimizing the synthesis of such glass ceramics by selecting the optimal ratio of RE ions for the realization of up-conversion luminescence. Previous studies of germanium–gallium glasses with Tm³⁺/Ho³⁺ ions indicate a maximum efficiency of up-conversion luminescence of 63% at an initial relative concentration of oxides of 70 Tm₂O₃/15 Ho₂O₃ [21]. It is known that the formation of luminescent nanoparticles in silicate composite systems is associated with the chemical processes between oxides of RE elements and components of the glass matrix [5,14]. However, the structural mechanisms of nanoparticle formation in the glass matrixes are studied less.

It is known that the effectiveness of up-conversion luminescence correlates with the nanoparticle structural characteristics, and the growth of nanoparticles depends on the conditions of glass thermal treatment [14]. From the position of the broad peak on the small-angle neutron scattering curves, it is possible to roughly estimate a shift in the average characteristic distance between clusters in the glass ceramics. Those distances increase by factors of 2–3, which can indicate an increase in the spacing between clusters in the glasses [14,18]. Taking into account the practical aspect of developing glass ceramics based on mixed oxide–fluoride glass matrixes as well as the interest in up-conversion luminescent materials, our work is directed to studying the structural aspects of the formation of nanoparticles containing Tm³⁺ and Ho³⁺ ions in mixed oxyfluoride glasses using small-angle X-ray scattering and X-ray diffraction methods.

2. Materials and Methods

The main problem in the development of transparent glass ceramic materials is the optimization of the initial glass composition, which, on the one hand, imparts high spectral luminescence properties, and, on the other hand, the stability of the vitreous state upon the introduction of fluorides and oxides of different RE elements with molar contents of several percent [5,14,17]. A small addition of thulium oxide improves the color properties of the up-conversion luminescence. The Ho^{3+} and Tm^{3+} ions have been chosen because this joint activation may enhance the color characteristics of the luminescence of the glass ceramics due to the diversity of possible mechanisms of excitation of up-conversion luminescence with the participation of pairs of ions $\text{Ho}^{3+}\text{-Tm}^{3+}$. The parent glass matrix is the mixed oxyfluoride vitreous system $2.2\text{SiO}_2\text{-}1.3\text{GeO}_2\text{-}6.9\text{PbO}\text{-}7.6\text{PbF}_2\text{-}2\text{CdF}_2\text{-}x\text{Ho}_2\text{O}_3\text{-}y\text{Tm}_2\text{O}_3$. The introduction of Ho_2O_3 and Tm_2O_3 oxides in a certain molar range was performed (Table 1). The selected concentration range of Ho_2O_3 corresponds to the maximum efficiency of up-conversion luminescence in similar glasses [21,23]. Structural studies of glasses doped with a variety of optically active nanoparticles are quite complex tasks due to the possible interaction between the nanoparticle elements and the vitreous material. A lead-containing glass matrix has been chosen to provide the light fusibility of the vitreous system. In particular, the introduction of reagents PbO and PbF_2 as glass-formers is a source of components for PbF_2 nanocrystal formation at lower temperatures of ~ 400 °C and a reduction of the temperature of glass synthesis to 900 °C. CdF_2 is an additional source of fluorine. It should be noted that in the first step, thoroughly mixed components of glass were fritted to reduce the evaporation of fluorine.

Table 1. Concentration of rare-earth oxides. The oxides concentrations are presented in the molar percent.

Sample Label	Ho_2O_3	Tm_2O_3
N1	0.6	–
N2	0.08	0.8
N3	0.4	0.8
N4	0.6	0.8
N5	–	0.8

The synthesis of glass was performed using traditional technology by melting a mixture that was prepared from pure chemical reagents. All reagents were mixed in corresponding proportions and homogenized by milling. The thoroughly mixed charge was placed into the corundum crucibles, which were put into an electric furnace. The synthesis of glasses was performed at a temperature of 950 °C, with exposure at maximum temperature for 30 min. The short period of 30 min is sufficient to complete the homogenization and refining of the glass sample. Glass components are fritted to reduce the evaporation of fluorine. We believe that the fluorine evaporation is less because the studied glass is fusible.

The glasses were annealed in the electric muffle furnace at 300 °C for 3 h. The X-ray diffraction data have confirmed the amorphous nature of the obtained glass materials. The glasses were heat-treated at 350 °C for 30 h + 360 °C for 50 h in order to form the PbF_2 nanoparticles [5,14].

Small-angle X-ray scattering (SAXS) is a useful technique for nanoscale structural characterization of glass materials [24,25]. In SAXS, structural and spatial information is indirectly obtained from the scattering intensity in the spectral domain, known as the reciprocal space [26]. Therefore, characterizing the structure requires solving the inverse problem of finding a plausible structure model that corresponds to the measured scattering intensity. Small-angle X-ray scattering experiments were performed with a Xeuss 3.0 instrument (XENOCSS SAS, Grenoble, France). The radiation was generated by a GeniX3D source (Mo-K α edge, $\lambda = 0.71078$ Å). Small-angle X-ray scattering curves were obtained using an Eiger2 detector at different sample-detector distances from 1 to 4 m. The thickness of the glass samples was 1 mm. The SAXS data were corrected for empty container data.

The analysis of small-angle scattering data was performed in the software package SasView (Version 5.0.6) [27].

The crystalline phase of the up-conversion luminescent nanoparticles in the glass matrix was studied using the X-ray diffraction method with the same Xeuss 3.0 device in diffraction mode, with the detector position at a distance of 0.5 m from the sample. We assumed that the crystal phase relates to the cubic phase of β -PbF₂ with space group $Fm\bar{3}m$ [5,15].

3. Results

The SAXS curves of the studied glass materials are shown in Figure 1. The scattered intensity was detected as a function of the momentum transfer modulus $q = (4\pi/\lambda)\sin\theta$, where θ is the scattering angle and λ is the incident X-ray wavelength [25]. The obtained curves for all samples are similar and have a typical shape for disordered glass systems [5,14,24]. There are small changes in the degree of slope of the curves and their shape, which may correspond to a change in the fractal dimensions of scattering objects. Figure 1b shows the Guinier plots $\{\ln(I(q)), q^2\}$, which provide the radius of inertia R_g of the scatterers [24,25]. The glass sample behavior exhibits a non-linear trend towards low q , where aggregation is detected by an upward curve, whereas a downward curve will be typical of particle repulsion [24]. It can be seen that, with an increase in the content of thulium oxide Tm₂O₃, there are noticeable changes in the Guinier graphs, which may indicate a clustering or aggregation of smaller particles [23,24]. On the other hand, the model of several scatters will be correct [5,14]. In this model, when the content of oxides increases, an increase in the average size of large particles or aggregates is expected. Therefore, to analyze the SAXS data, we used a two-particle model, which postulates the contribution to SAXS curves from luminescent nanoparticles, most likely PbF₂:Tm-Ho [14], and from fluctuations in density inside the glass matrix [10]. This model has been used previously in studies of other glass systems [5,14,28].

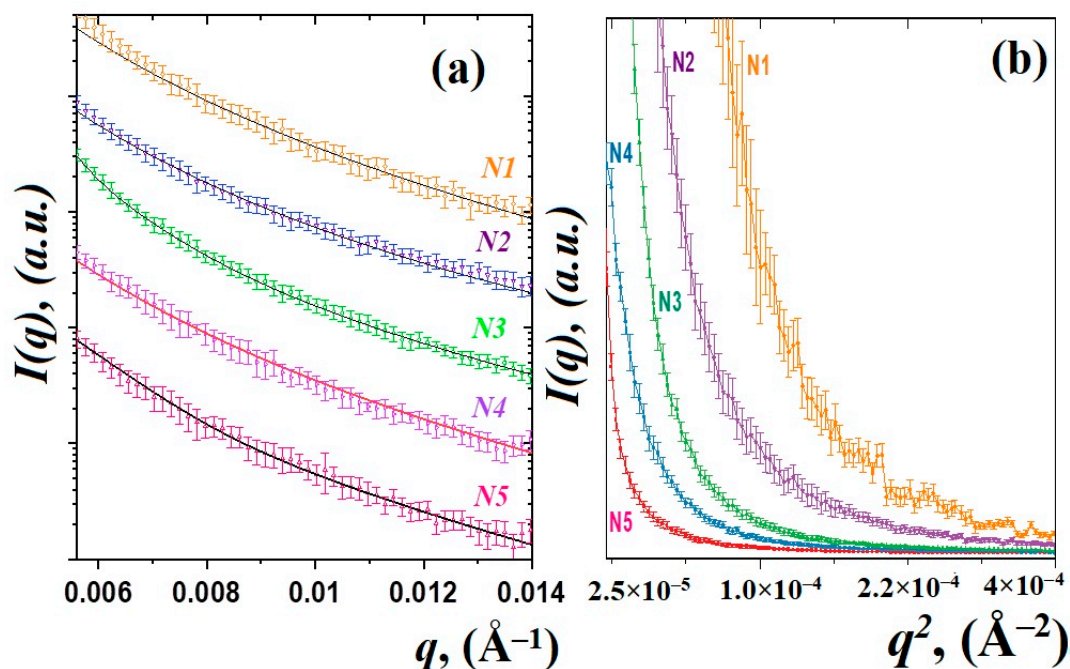


Figure 1. SAXS curves of the studied glass materials and their approximation by function (a). Guinier plots for the SAXS experimental data (b).

Therefore, the obtained SAXS curves were approximated by using the exponential-power law model of Beaucage [29,30]. Those approaches to the analysis of small-angle scattering describe scattering from complex systems that contain multiple levels of related

structural features. It should be noted that even in the absence of nanoparticles in the glass matrix, glass density heterogeneities of different natures can act as scattering objects. The scattering intensity from a system of two scatters is represented by the following expression:

$$I(q) = G_1 \exp\left(\frac{-q^2 R_{g1}^2}{3}\right) + B_1 \exp\left(\frac{-q^2 R_{g1}^2}{3}\right) \left(\frac{1}{q_1^*}\right)^{P_1} + G_2 \exp\left(\frac{-q^2 R_{g2}^2}{3}\right) + B_2 \exp\left(\frac{-q^2 R_{g2}^2}{3}\right) \left(\frac{1}{q_2^*}\right)^{P_2}, \quad (1)$$

where the coefficients G_1 , G_2 , B_1 and B_2 and the degrees at exponents P_1 and P_2 are the fitted parameters for the first and second structural levels, respectively. The radius of gyration R_{g1} and R_{g2} correspond to the main parameters of the sizes of scattering objects. The functions q_1^* and q_2^* in a power function are normalized as:

$$q_1^* = \frac{q}{\left[\operatorname{erf}\left(\frac{k_1 q R_{g1}}{\sqrt{6}}\right)\right]^3}, \quad q_2^* = \frac{q}{\left[\operatorname{erf}\left(\frac{k_2 q R_{g2}}{\sqrt{6}}\right)\right]^3} \quad (2)$$

where k_1 and k_2 are empirical coefficients. The values of the gyration radius R_{g1} and R_{g2} are correlated with fluctuations in the density of glass [10] and with the PbF_2 :Tm-Ho nanoparticles, respectively.

The calculated values of the power-law exponents P_1 and P_2 obtained from fitting SAXS data by using Equation (1) are associated with the fractal dimension of the nanostructured system [24,31]. A power-law exponent in the range between 1 and 3 corresponds to mass fractals [24,25], one between 3 and 4 indicates surface fractals and between 4 and 6 is a diffuse surface. It is evident that the fractal dimensions of the observed nanoparticles PbF_2 :Tm-Ho vary slightly within the range $P_1 = 3.0 \div 3.6$, which can correspond to some estimated nanoparticles with a smooth, sharp interface [24,31]. At the same time, the slope degree P_2 of the SAXS curve related to the density fluctuations does not exceed 3, which corresponds to the mass fractals. Large regions of density fluctuations of the glass material are formed in the glass matrix and are governed by the essential features of the chemical interaction of the glass components [10,14]. The observed density fluctuations of the glass material can serve as nucleation centers [15] for the nanostructured particles PbF_2 :Tm-Ho.

The results of the approximation of the experimental data by the function (1) are shown in Figure 1a. The calculated size variation of the density fluctuations and formed nanoparticles is shown in Figure 2a. It can be noted that, in heat-treated glasses doped with thulium and holmium ions, the nanoparticles of 42–46 nm in size (Figure 2b) are formed in a spherical approximation, where the diameter of the nanoparticles is calculated as $D = 2(5/3)^{1/2} R_g$ and the average sizes of density fluctuations in the glass matrix grow from 204(2) nm for sample N1 to 324(3) nm for sample N5.

Interestingly, as the relative concentration of $\text{Tm}_2\text{O}_3/\text{Ho}_2\text{O}_3$ oxides increases, both the average size of nanoparticle clusters and the glass density fluctuations are growing. It can be explained that rare-earth ions are localized not only in nanoparticles but also in the glass matrix in the form of oxides [5,14]. In order to estimate the average size ranges of both glass density fluctuations and nanoparticles, approximations of SAXS data using functions (1) and (2) were used. The SAXS technique is much superior when considering the determination of the size distribution on a several-nanometer length scale for opaque solutions and for solid specimens [31].

Scattering comprises not only contributions from the regularity of the space-filling ordering of particles but also from a single particle. The particle scattering can be mathematically formulated depending on the type of particle shape. In block copolymer microdomain systems, the Gauss distribution of the particle size has been assumed [24,31]. Only recently has direct determination of the discrete size distribution been available by fitting the theoretical scattering function to the experimentally obtained SAXS profile [27].

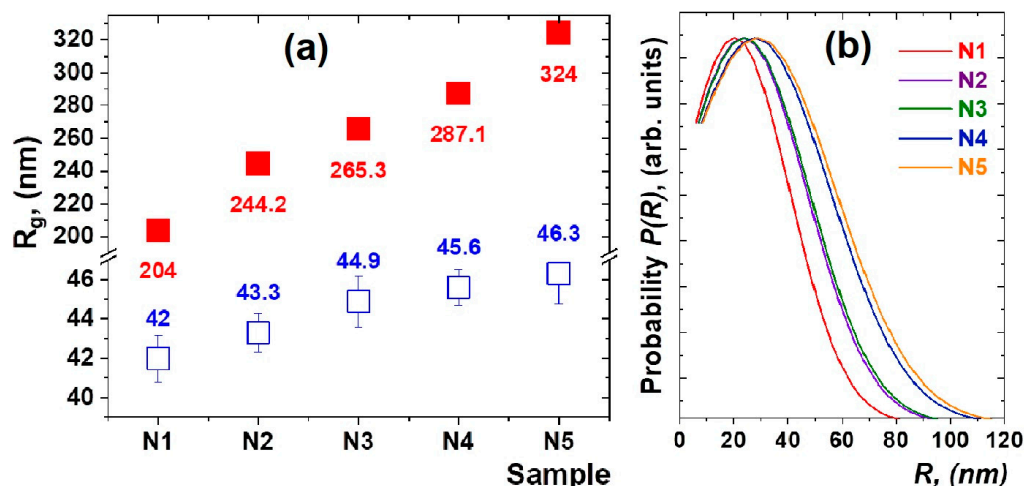


Figure 2. The values of the gyration radii Rg1 (red close squares) of the density fluctuations and Rg2 (blue open square) of nanoparticles, which were calculated from the analysis of the SAXS data for the studied glass materials. The obtained values are normalized to the corresponding values for N1 sample (a). The distribution of average sizes of nanoparticles in the studied glass samples obtained by Equations (3) and (4) (b).

The paired distribution function of nanoparticles of intermediate size, having a finite maximum size D_{max} , was approximated by a linear combination of a finite number of N cubic B-splines uniformly distributed in the range from 0 to D_{max} :

$$\rho(r) = \sum_{i=1}^N a_i \phi_i(r) \tag{3}$$

where a_i is the coefficient of the i -th cubic B-spline, $\phi_i(r)$ [31,32]. The upper limit of the values of the parameter r , included in the inverse Fourier transform, was chosen in such a way that the function $\rho(r)$ smoothly tends to 0 for large values of r . Using the above-mentioned mathematical apparatus, it is possible to estimate the paired distribution function for a system of non-interacting aggregates. Based on the obtained dependencies $\rho(r)$, it is possible to determine the radius of gyration R_g , which characterizes the size of intermediate nanoparticles:

$$R_g = \left[\frac{\int_0^D r^2 p(r) dr}{\int_0^D p(r) dr} \right]^{1/2} \tag{4}$$

The results of the analysis are shown in Figure 2b. It can be seen that the average size of nanoparticles in the spherical approximation [31,32] shifts to the region of large sizes, although the width of the distribution does not change significantly. Interestingly, the slope of the SAXS curves practically does not change, and its average value is $\alpha = -5.1(5)$. This indicates that the fractal dimensionality and morphology of the nanostructured components of the heat-treated glasses are preserved.

As an important aspect, the structural mechanisms of $PbF_2:Tm-Ho$ nanoparticle formation can also be explained by the detection of the crystalline or amorphous state of the luminescent nanoparticles. X-ray diffraction patterns for the studied glass samples are shown in Figure 3. All diffraction patterns obtained have a typical shape for scattering from amorphous materials. However, on the X-ray diffraction pattern corresponding to samples N2, N3 and N4, the appearance of several diffraction peaks is observed. The positions of the observed diffraction peaks correspond to the cubic structure with $Fm\bar{3}m$ symmetry and indicate the PbF_2 phase [5,14]. We believe that the rare-earth ions became embedded in crystals of PbF_2 because the unit cell parameter of this phase changes slightly with increasing thulium and holmium oxide concentration, which indicates the entry of Ho^{3+}

and Tm^{3+} ions into the crystal structure of the luminescent nanoparticle $\text{PbF}_2\text{:Tm-Ho}$. Here, it is declared that the spectral characteristics of up-conversion luminescence correspond to those related to the cubic crystal structure of PbF_2 crystal [4,33].

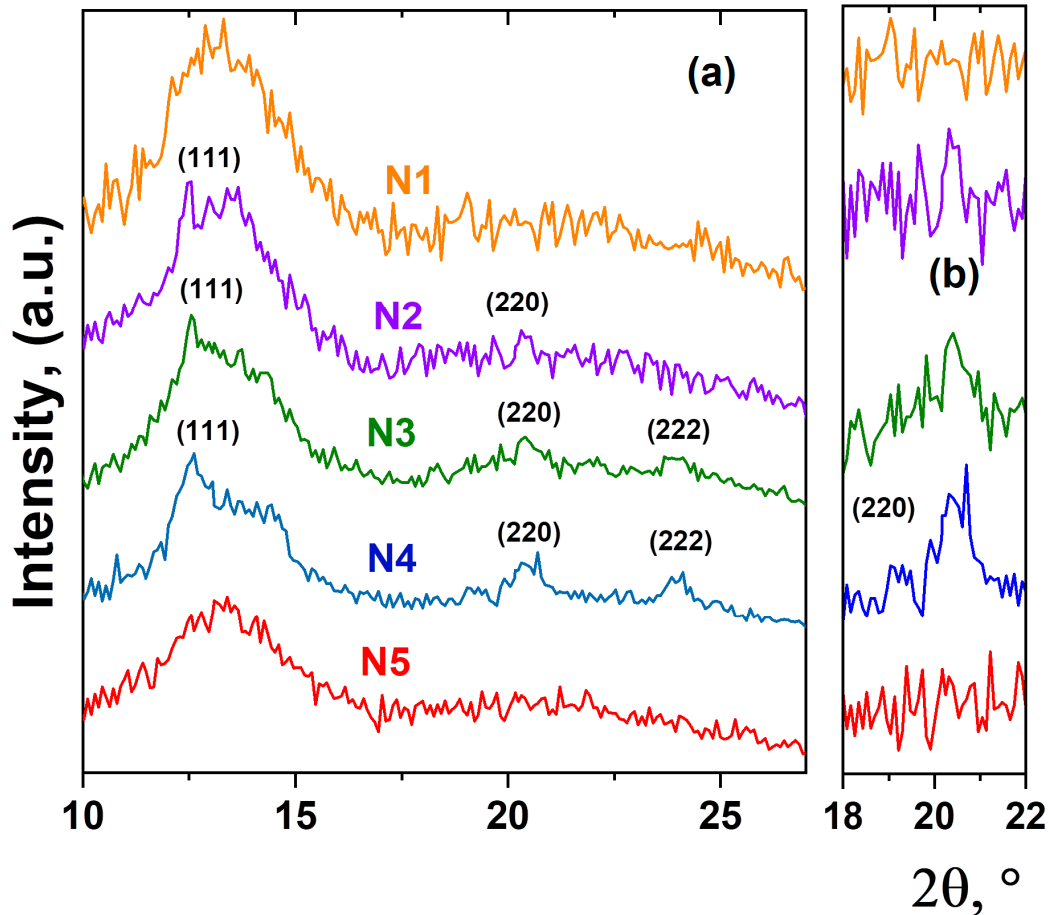


Figure 3. X-ray diffraction patterns of heat-treated glasses. The diffraction peaks of cubic phase $\text{PbF}_2\text{:Tm-Ho}$ are indicated by Miller indices (a). The enlarged section of the diffraction pattern in scattering angle range $18\text{--}22^\circ$, where the diffraction reflex (220) of the cubic phase $\text{PbF}_2\text{:Tm-Ho}$ is detected (b).

Based on the obtained experimental data, the following structural mechanism of nanoparticle formation in the heat-treated glass can be proposed. As previously assumed [5,10,19], the density fluctuations in the glass materials can serve as the nucleation centers for the oxide nanoparticles $\text{PbF}_2\text{:Tm-Ho}$. At low concentrations of the initial oxides Tm_2O_3 and Ho_2O_3 , complex amorphous nanostructured structures, or aggregates, are formed. The nanoparticles form complex branching structures consisting of regular fractal arrangements of clusters inside the glass material. With increasing oxide concentration, the formation of a crystalline phase of PbF_2 nanoparticles with changes in the local environment of the glass matrix is observed. These crystallized PbF_2 nanoparticles are a host system for rare-earth Tm^{3+} and Ho^{3+} ions, whose entry into the cubic crystal lattice of PbF_2 provides conditions for up-conversion luminescence [4,5].

4. Conclusions

The structural features of nanoparticle formation in heat-treated mixed oxyfluoride glasses have been studied using small-angle X-ray scattering and X-ray diffraction methods. It has been established that nanoparticles, presumably $\text{PbF}_2\text{:Tm-Ho}$ with sizes of 42–46 nm, are formed at the selected heat-treatment mode. An increase in the average size of the density fluctuations in glass from 204(2) to 324(3) nm is observed. With an increase in

the concentration of Ho_2O_3 and Tm_2O_3 oxides, the average sizes of nanoparticles and the sizes of local areas of density fluctuations both increased. The obtained structural information will be useful for the analysis of the optical properties of nanostructured up-conversion-luminescent glass ceramics.

Author Contributions: Conceptualization, E.T. and S.D.; methodology, S.D. and K.P.; formal analysis, S.D.; investigation, S.D. and K.P.; data curation, S.D. and K.P.; writing—original draft preparation, S.K. and E.T.; writing—review and editing, S.K. and E.T.; visualization, S.D. and S.K.; supervision, D.K.; project administration, D.K. and E.T. All authors have read and agreed to the published version of the manuscript.

Funding: This research did not receive any specific grant from funding agencies in the public, commercial, or not-for-profit sectors.

Informed Consent Statement: Not applicable.

Data Availability Statement: Not applicable.

Conflicts of Interest: The authors declare no conflict of interest.

References

1. Probst, J.; Dembski, S.; Milde, M.; Rupp, S. Luminescent nanoparticles and their use for in vitro and in vivo diagnostics. *Expert Rev. Mol. Diagn.* **2012**, *12*, 49–64. [[CrossRef](#)] [[PubMed](#)]
2. Fares, H.; Elhouichet, H.; Gelloz, B.; Férid, M. Silver nanoparticles enhanced luminescence properties of Er^{3+} doped tellurite glasses: Effect of heat treatment. *J. Appl. Phys.* **2014**, *116*, 123504. [[CrossRef](#)]
3. Tikhomirov, V.K.; Furniss, D.; Reaney, I.M.; Beggiora, M.; Ferrari, M.; Montagna, M.; Rolli, R. Fabrication and characterization of nanoscale, Er^{3+} -doped, ultratransparent oxyfluoride glass ceramic. *Appl. Phys. Lett.* **2002**, *81*, 1937–1939. [[CrossRef](#)]
4. Loiko, P.A.; Rachkovskaya, G.E.; Zakharevich, G.B.; Kornienko, A.A.; Dunina, E.B.; Yasukevich, A.S.; Yumashev, K.V. Cooperative up-conversion in Eu^{3+} , Yb^{3+} -doped SiO_2 - PbO - PbF_2 - CdF_2 oxyfluoride glass. *J. Non-Cryst. Solids* **2014**, *392–393*, 39–44. [[CrossRef](#)]
5. Kichanov, S.E.; Kozlenko, D.P.; Gorshkova, Y.E.; Rachkovskaya, G.E.; Zakharevich, G.B.; Savenko, B.N. Structural studies of nanoparticles doped with rare-earth ions in oxyfluoride lead-silicate glasses. *J. Nanopart. Res.* **2018**, *20*, 54. [[CrossRef](#)]
6. Trusova, E.E.; Bobkova, N.M.; Gurin, V.S. Nature of color centers in silicate glasses with additions of cerium and titanium oxides. *Glass Ceram.* **2009**, *66*, 9–13. [[CrossRef](#)]
7. Bondar, I.V.; Gurin, V.S.; Solovey, N.P.; Molochko, A.P. Formation and optical properties of CuInTe_2 nanoparticles in silicate matrices. *Semiconductors* **2007**, *41*, 939–945.
8. Sigae, V.N.; Golubev, N.V.; Usmanova, L.Z.; Stefanovich, S.Y.; Pernice, P.; Fanelli, E.; Aronne, A.; Champagnon, B.; Califano, V.; Vouagner, D.; et al. On the nature of the second-order optical nonlinearity of nanoinhomogeneous glasses in the Li_2O - Nb_2O_5 - SiO_2 system. *Glass Phys. Chem.* **2006**, *33*, 97–105. [[CrossRef](#)]
9. Zhang, Y.; Wang, Y. Nonlinear optical properties of metal nanoparticles: A review. *RSC Adv.* **2017**, *7*, 45129–45144. [[CrossRef](#)]
10. Kichanov, S.E.; Islamov, A.K.; Samoilenko, S.A.; Kozlenko, D.P.; Belushkin, A.V.; Gurin, V.S.; Shevchenko, G.P.; Trusova, E.E.; Bulavin, L.A.; Savenko, B.N. Studying the structural features of oxide nanoclusters of cerium and titanium in a silicate glass by means of the small-angle neutron scattering. *J. Surf. Investig.* **2014**, *8*, 98–103. [[CrossRef](#)]
11. Samoilenko, S.A.; Kichanov, S.E.; Belushkin, A.V.; Kozlenko, D.P.; Garamus, V.M.; Gurin, V.S.; Trusova, E.A.; Shevchenko, G.P.; Rakhmanov, S.K.; Bulavin, L.A.; et al. Study of Structural Aspects of the Cluster Formation in Silicate Glasses Doped with Cerium and Titanium Oxides by Small-Angle Neutron Scattering. *Phys. Solid State* **2011**, *53*, 2431–2434. [[CrossRef](#)]
12. Godard, A. Infrared (2–12 μm) solid-state laser sources: A review. *Comptes Rendus Phys.* **2007**, *8*, 1100–1128. [[CrossRef](#)]
13. Nishibu, S.; Nishio, T.; Yonezawa, S.; Takashima, M. Fluorescence enhancement of oxide fluoride glass co-doped with TbF_3 and SmF_3 . *J. Lumin.* **2007**, *126*, 365–370. [[CrossRef](#)]
14. Kichanov, S.E.; Gorshkova, Y.u.E.; Rachkovskaya, G.E.; Kozlenko, D.P.; Zakharevich, G.B.; Savenko, B.N. Structural evolution of luminescence nanoparticles with rare-earth ions in the oxyfluoride glass ceramics. *Mater. Chem. Phys.* **2019**, *237*, 121830–121837. [[CrossRef](#)]
15. Golubkov, V.V.; Bogdanov, V.N.; Pakhnin, A.Y.; Solovyev, V.A.; Zhivaeva, E.V.; Kabanov, V.O.; Yanush, O.V.; Nemilov, S.V.; Kisiuk, A.; Soltwisch, M.; et al. Microinhomogeneities of glasses of the system PbO - SiO_2 . *J. Chem. Phys.* **1999**, *110*, 4897–4906. [[CrossRef](#)]
16. Auzel, F. Up-conversion and anti-Stokes processes with d and f ions in solids. *Chem. Rev.* **2004**, *104*, 139–174. [[CrossRef](#)]
17. Loiko, P.A.; Rachkovskaya, G.E.; Zakharevich, G.B.; Skoptsov, N.A.; Yumashev, K.V. Luminescence of Oxyfluoride Glasses Containing Yb^{3+} - RE^{3+} Ions. *Glass Ceram.* **2016**, *73*, 9–13. [[CrossRef](#)]
18. Guinhos, F.C.; Nóbrega, P.C.; Santa-Cruz, P.A. Compositional dependence of up-conversion process in Tm^{3+} - Yb^{3+} codoped oxyfluoride glasses and glass-ceramics. *J. Alloys Compd.* **2001**, *323–324*, 358–361. [[CrossRef](#)]

19. Dwivedi, Y.; Thakur, S.N.; Rai, S.B. Study of frequency upconversion in $\text{Yb}^{3+}/\text{Eu}^{3+}$ by cooperative energy transfer in oxyfluoroborate glass matrix. *Appl. Phys.* **2007**, *B 89*, 45–51. [[CrossRef](#)]
20. Maciel, G.S.; Biswas, A.; Prasad, P.N. Infrared-to-visible Eu^{3+} energy up-conversion due to cooperative energy transfer from an Yb^{3+} ion pair in a sol-gel processed multicomponent silica glass. *Opt. Commun.* **2000**, *178*, 65–69. [[CrossRef](#)]
21. Kochanowicz, M.; Zmojda, J.; Miluski, P.; Baranowska, A.; Leich, M.; Schwuchow, A.; Jäger, M.; Kuwik, M.; Pisarska, J.; Pisarsk, W.A.; et al. $\text{Tm}^{3+}/\text{Ho}^{3+}$ co-doped germanate glass and double-clad optical fiber for broadband emission and lasing above 2 μm . *Opt. Mater. Express* **2019**, *9*, 1450–1458. [[CrossRef](#)]
22. Dwaraka Viswanath, C.S.; Babu, P.; Martín, I.R.; Venkatramu, V.; Lavín, V.; Jayasankar, C.K. Near-infrared and upconversion luminescence of Tm^{3+} and $\text{Tm}^{3+}/\text{Yb}^{3+}$ -doped oxyfluorosilicate glasses. *J. Non-Cryst. Solids*. **2018**, *507*, 1–10. [[CrossRef](#)]
23. Richards, B.; Shen, S.; Jha, A.; Tsang, Y.; Binks, D. Infrared emission and energy transfer in Tm^{3+} , $\text{Tm}^{3+}\text{-Ho}^{3+}$ and $\text{Tm}^{3+}\text{-Yb}^{3+}$ -doped tellurite fibre. *Opt. Express*. **2007**, *15*, 6546–6551. [[CrossRef](#)]
24. Brumberger, H. *Modern Aspects of Small-Angle Scattering*; Springer: Dordrecht, The Netherlands, 1995. [[CrossRef](#)]
25. Svergun, D.I. Determination of the regularization parameter in indirect-transform methods using perceptual criteria. *J. Appl. Cryst.* **1992**, *25*, 495–503. [[CrossRef](#)]
26. Röding, M.; Tomaszewski, P.; Yu, S.; Borg, M.; Rönnols, J. Machine learning-accelerated small-angle X-ray scattering analysis of disordered two- and three-phase materials. *Front. Mater.* **2022**, *9*, 956839–956852. [[CrossRef](#)]
27. SasView for Small-Angle Scattering Analysis. Available online: <http://www.sasview.org/> (accessed on 20 May 2019).
28. Rutkauskas, A.V.; Gorshkova, Y.E.; Gurin, V.S.; Kichanov, S.E.; Kozlenko, D.P.; Alekseenko, A.A. Investigation of Silicate Sol-Gel Glass Doped with Cu_2Se and Eu Nanoparticles by Small-Angle Neutron Scattering and Atomic-Force Microscopy. *J. Surf. Investig. X-Ray Synchrotron Neutron Tech.* **2022**, *16*, 1094–1100. [[CrossRef](#)]
29. Beaucage, G. Approximations leading to a unified exponential/power-law approach to small-angle scattering. *J. Appl. Cryst.* **1995**, *28*, 71–728. [[CrossRef](#)]
30. Hammouda, B. Analysis of the Beaucage model. *J. Appl. Cryst.* **2010**, *43*, 1474–1478. [[CrossRef](#)]
31. Teixeira, J. Small-angle scattering by fractal systems. *J. Appl. Cryst.* **1988**, *21*, 781–785. [[CrossRef](#)]
32. Schmidt, P.W. Small-angle scattering studies of disordered, porous and fractal systems. *J. Appl. Cryst.* **1991**, *24*, 414–435. [[CrossRef](#)]
33. Bevan, D.J.M.; Strähle, J.; Greis, O. The crystal-structure of tveitite, an ordered yttrifluorite mineral. *J. Solid State Chem.* **1982**, *44*, 75–81. [[CrossRef](#)]

Disclaimer/Publisher’s Note: The statements, opinions and data contained in all publications are solely those of the individual author(s) and contributor(s) and not of MDPI and/or the editor(s). MDPI and/or the editor(s) disclaim responsibility for any injury to people or property resulting from any ideas, methods, instructions or products referred to in the content.